Approach to the development of a model to quantify the quality of tendon localization in concrete using ultrasound

Stefan Küttenbaum [1*], *Stefan* Maack [1], and *Alexander* Taffe [2]

[1] Bundesanstalt für Materialforschung und -prüfung (BAM), Unter den Eichen 87, 12205 Berlin, Germany
[2] HTW Berlin – University of Applied Sciences, Wilhelminenhofstraße 75a,12459 Berlin, Germany

Abstract. Each engineering decision is based on a number of more or less accurate information. In assessment of existing structures, additional relevant information collected with on-site inspections facilitate better decisions. However, observed data basically represents the physical characteristic of interest with an uncertainty. This uncertainty is a measure of the inspection quality and can be quantified by expressing the measurement uncertainty. The internationally accepted rules for calculating measurement uncertainty are well established and can be applied straightforwardly in many practical cases. Nevertheless, the calculations require the occasionally time-consuming development of an individually suitable measurement model. This contribution attempts to emphasize proposals for modelling the non-destructive depth measurement of tendons in concrete using the ultrasonic echo technique. The proposed model can serve as guideline for the determination of the quality of the measured information in future comparable inspection scenarios.

1 Introduction

In assessment of structures, the values and the validity of computed failure probabilities significantly depend on the considered information. With regard to existing structures, it is not uncommon, that necessary sources of information (such as as-built plans or structural analyses performed in the design stage) are missing, incomplete or illegible [1–3]. In addition, doubts about the available information may arise. However, missing or questioned information in assessment of existing structures can be verified by inspection or testing on-site [4, 5]. Although it is well known that the ground penetrating radar or the ultrasonic echo technique can be used for clarification of the inner structure of concrete components, cf. e.g. [6], the quality of the testing results is in many cases not comparably specified. This is an obstacle in that the quality of the measured information needs to be known and its comparability must be ensured in order to be able to utilize testing results in assessment models or digital representations. When measurement uncertainties have been stated, measuring data, that initially represented a characteristic of interest (e. g. a physical quantity) only uncertainly and more or less well, in turn, enable better engineering decisions. These include but are not limited to more realistic assessments of structural reliability or a more targeted planning of necessary measures such as use restrictions or maintenance work.

The rules to calculate the measurement uncertainty provided in the Guide to the Expression of Uncertainty in Measurement (GUM) are internationally accepted in metrology [7–9]. While the calculation itself can be performed straightforwardly in many practical cases, the modelling of the measurement, which is principally necessary, requires extensive knowledge of the entire measuring process and may be too laborious in practice. Therefore, this paper contains a developed measurement model that was used to compute measurement results (including uncertainties) describing mounting depths of tendons in a prestressed concrete bridge using ultrasonic echo. This model is, in principle, only valid for this individual case, but may be utilized as orientation for comparable future measurement scenarios. Further, it can be used to estimate the dimension of the achievable measurement uncertainties in non-destructive as-built plan reconstruction using ultrasound. In conclusion, it is shown how the incorporation of non-destructively measured and quality-assured inner geometrical dimensions, i.e., the tendon position, into probabilistic assessment can influence structural reliability. General guidance on the measurement model development has been recently published in [10].

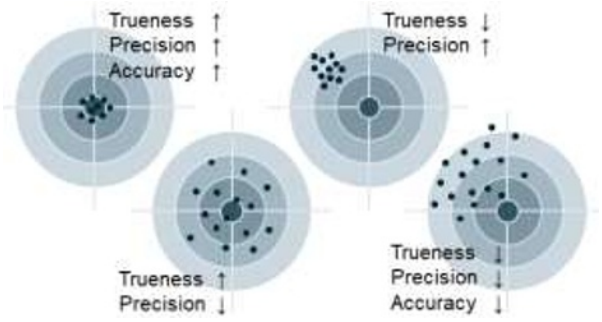

Fig. 1. Targets to visualize the qualitative measures accuracy, expressed by trueness and precision (arrows indicate the qualitative extent of measures; centre represents a reference value). Extracted from [11], translated; acc. to [12, 13].

* Corresponding author: stefan.kuettenbaum@bam.de

2 Measurement uncertainty

Results of a measurement cannot be predicted certainly. The expression of a measurement result requires that a measured quantity value is found, which represents the quantity of interest (measurand). Such a measured value can be regarded as an estimated value of the measurand, which is generally only an approximation of the purely theoretical true value(s). Even if the measurements are carried out meticulously careful, it is unavoidable, that observations scatter randomly. Thus, there is basically an uncertainty with respect to the measured value, which we can call measurement uncertainty. This is not to be understood as a result of mistakes, but as a measure of the quality of the measurement, that must be adequately quantified and expressed.

Measurement uncertainty establishes confidence in measurement, ensures the comparability of results, and states the *quality* of the information measured, that is, *trueness* and *precision*. The *accuracy* can be regarded as an umbrella term for precision and trueness (see Fig. 1). High precision is achieved when the random errors are small (low variability of observations). Provided, that systematic errors have been corrected, the precision is inversely proportional to the measurement uncertainty. It should be considered, that precise but incorrect (not true) measurements pose the risk of misinterpretation of measured values since a high precision may suggest the impression of a high accuracy, which may lead to an unintentional neglection of existing systematic effects (cf. Fig. 1, third target from the left). Such systematic measurement errors have to be identified and corrected when calculating measurement uncertainty, e.g., using reference values.

The calculation of measurement uncertainties acc. to the GUM [7] is summarized in Figure 2. The central part is to find a suitable model of the measurement, which consists of a defined measurand Y, the identified and (usually stochastically) modelled input quantities X_i and the model equation, that may be expressed in an explicit form as $Y = f(X_i)$. The input quantities X_i influence the outcome of a measurement (often unfavourably as they contribute to measurement uncertainty) and / or may be necessary to compute the measurement result.

Following the measurement model development, the calculation rules of the GUM can be applied in many practical cases straightforwardly. The rules can be found for example in [7, 12] and in excepts in Figure 2. They are delimited in this paper. The measurement result can then be stated by the measured quantity value $\hat{y}$ and the attributed combined standard measurement uncertainty $u(\hat{y})$, which expresses the measurement uncertainty as a standard deviation [14]. Some disciplines prefer the use of a coverage *interval* $y \pm ku(\hat{y})$ containing the "set of true (…) values of a measurand" [14] with a defined probability p (cf. Fig. 2; for comparison, see Fig. 3).

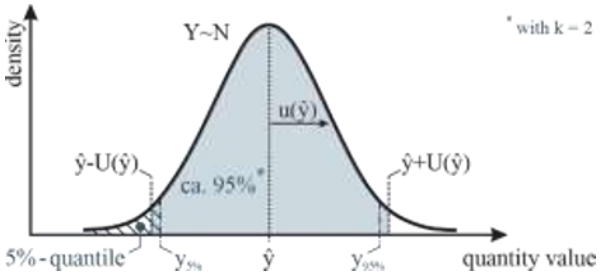

Fig. 3. Combined standard measurement uncertainty $u(\hat{y})$, expanded measurement uncertainty $U(\hat{y}) = ku(\hat{y}) \triangleq 2u(\hat{y})$, measured quantity value $\hat{y}$, and quantile values $y_{p[\%]}$.

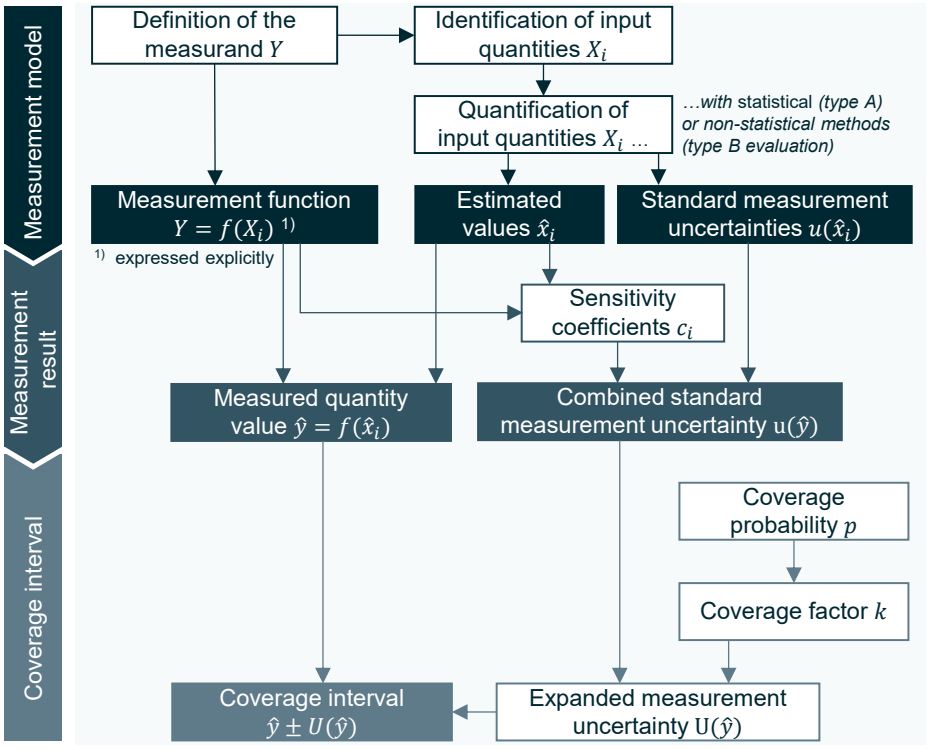

$$\hat{x} = \bar{x} - b = \left(\frac{1}{n}\sum_{i=1}^{n} x_i\right) - b$$

(in case of type A evaluation; b ≡ bias)

$$u(\hat{x}) = \sqrt{\frac{1}{n(n-1)}\sum_{i=1}^{n}(x_i - \bar{x})^2}$$

(in case of type A evaluation)

$$c_i = \left[\frac{\partial f(X_1, \ldots, X_n)}{\partial X_i}\right]_{X_1=\xi_1,\ldots,X_n=\xi_n}$$

(partial derivates at estimated values $\hat{x}_i$)

$$u(\hat{y}) = \sqrt{\sum_{i=1}^{n} c_i^2 u^2(\hat{x}_i)}$$

(in case of uncorrelated input quantities)

$$U(\hat{y}) = k \cdot u(\hat{y})$$

(value of k also depends on distr. type of Y)

Fig. 2. Flowchart: Calculation of measurement uncertainties according to JCGM 100:2008 (GUM) for a single, normally distributed measurand. Extracted from [11], translated, formulae added; acc. to [15, 16].

3 The proposed model

3.1 Definition of the measurand

The presented measurement model was developed to quantify the uncertainty associated with the localization of transverse tendons in a prestressed concrete bridge in northern Germany during its assessment. The four spans yield a total length of approx. 96 m. The structure was built in 1980 and carries a federal highway. The slab-and-beam cross-section with its two main girders (see Fig. 4) is broader than 23 m. Further information about the structure and the reassessment are given in [17].

The quantity of interest is the mounting depth of a number of tendons in relation to the undersurface of the slab. The decisive cross-sections have been determined using Finite Element analyses. They were used to define the measuring area. The amount and the vertical position of the transverse tendons has been found to significantly influence structural reliability in SLS decompression, which had to be analysed in transverse bridge direction.

The non-destructive testing (NDT) was carried out using the ultrasound echo technique. Considering the small thickness of the tendon ducts and the findings in [18], the interface between the surrounding concrete and the mortar inside the ducts is defined as reflector at least for areas that have good grouting conditions. The shear waves were transmitted using a dual aperture shear wave DPC transducer array. The centre frequency is approx. f = 55 kHz. A scanner system developed at BAM was used for precise probe positioning.

Fig. 4. Photo of the investigated prestressed concrete bridge

3.2 Identification of input quantities

The measurand $Y = D_{Sp}$ is the depth position of the interface between concrete and grouting mortar of one tendon. The tendons are bonded post-tensioning. The measurand thus describes the mounting depth of the tendon duct. The lateral position in longitudinal (x) and transversal (y) bridge direction is basically attributed to such a position. The depth (z) is then considered as a sampling point describing the mounting depth of one particular tendon in a certain small area spanned in x- and y- direction. A number of sampling points can be used to interpolate the course of a tendon.

The measurand D_{Sp} is a function of input quantities, which are necessary to compute the result, contribute to measurement uncertainty, and / or describe biases. The identification of the input quantities considered relevant in the present case is briefly discussed in the following:

- ***Propagation velocity of the shear wave*** $\boldsymbol{C_T}$
  The sound velocity depends on the concrete density, dynamic modulus of elasticity, the Poisson's ratio, and boundary conditions such as the temperature [6, 19]. In view of concrete inhomogeneity, C_T must be determined individually (in this case as a function of a reference thickness and time of flights observed in volumes with properties comparable to the component of interest; see Eq. 2) to derive unbiased depth positions using Eq. 1.

- ***Time of flight for mounting depth determination*** $\boldsymbol{T}$
  Time of flight (TOF) used for depth measurement is a function of the displayed values and further quantities affecting the outcome of the testing, see Eq. 3.

- ***Unevenness of the measuring surface*** $\boldsymbol{D_{Sp,U}}$
  In ultrasonic testing on-site, the DPC transducers are pressed onto the concrete surface. The reference plane for specifying a depth position is assumed to be a plane measuring surface. Random errors from this reference may influence measured depth positions of reflectors.

- ***Reference thickness for velocity determination*** $\boldsymbol{D_{C_T}}$
  The uncertainty in the measurement of a reference thickness equals the combined standard measurement uncertainty calculated for the respective inspection or, if as-built drawings were used, may be quantified using permissible deviations according to the applicable code.

- ***Time of flights for velocity determination*** $\boldsymbol{T_{C_T,A}}$
  The time stamps extracted to determine C_T from the time signals that were acquired in an area with a known component thickness are gathered in the sample, i.e., the measuring series $\boldsymbol{t_{C_T,A}} = \left(t_{C_T,A,1}, \dots, t_{C_T,A,n}\right)^T$.

- ***Changes in pulse shape*** $\boldsymbol{T_{A,IF}}$
  Sound attenuation (scattering and absorption) and dispersion cause changes in the pulse shape depending on the travel path and frequency. This change in shape between the transmitted and received impulse leads to a shift of the time stamps within an echo (such as maxima, zero-crossings) in relation to the first arrival depending on aggregate diameter and concrete density [20–22].

- ***Offset (delay)*** $\boldsymbol{T_V}$
  TOF measurements aim to determine the amount of time it takes for a pulse to travel a certain distance within the measuring object. A recorded time signal additionally includes (at least in part) the time required to generate, transmit, and sample the signal. This offset needs to be estimated and corrected to find time zero.

- ***Limited resolution of the measuring scale*** $\boldsymbol{T_Z}$
  The resolution of the time axis in TOF measurement depends on the sampling rate (in this case $f_s = 1\ MHz$).

- ***Varying component temperatures $C_{T,T}$***

Different evaluations of the influence of temporal or spatial temperature changes of concrete components on the propagation velocity of the elastic wave can be found in the literature, e.g., [19, 23, 24].

- ***Varying component moisture $C_{T,F}$***

It was found that the moisture content of a measuring object may affect the propagation velocity [23, 25–27].

- ***Time of flights picked for depth measurement T_A***

The time stamps extracted from the time signals in a certain, small region limited in x- and y- directions are recorded in the measuring series $\boldsymbol{t_A} = \left(t_{A,1}, \dots, t_{A,n}\right)^T$.

- ***Competing points of reflection $T_{A,KS}$***

In case of bonded post-tensioning, the system *tendon* consists of duct, strands, and grouting; neglecting voids. If the tendon position is to be measured with ultrasound, there are multiple conceivable, closely spaced interfaces (in relation to the wavelength), all of which represent a potential reflection point since the (if intact) acoustically connected materials have different acoustic impedances.

- ***Spacing between transmitter and receiver T_{SE}***

The geometrical distance between transmitting and receiving probe must be considered since the travel path of the impulse is larger than twice the reflector depth in bistatic echo measurements.

- ***Unknown processes in the measuring system T_M***

Unknown processes inside the measuring equipment ("black box") can lead to random measurement errors.

3.3 Model equation

The Ishikawa diagram (see Figure 5) summarizes the identified input quantities which are considered relevant in the present case. The mathematical relationship can be formulated analogously to [15] as follows:

$$D_{Sp} = \frac{C_T T}{2} - D_{Sp,U} \quad \text{, where} \tag{1}$$

$$C_T = \frac{2D_{C_T}}{T_{C_T,A} - T_{A,IF} - T_V - T_Z} - C_{T,T} - C_{T,F} \quad \text{, and} \tag{2}$$

$$T = T_A - T_{A,KS} - T_{A,IF} - T_V - T_Z - T_{SE} - T_M \tag{3}$$

If the distribution of an input quantity does not only cover random errors, but also estimated systematic effects, the algebraic signs should be chosen carefully. The symbols used in Eqs. 1 - 3 are explained in Fig. 5.

Some of the identified uncertainty contributions can be minimized by an appropriate design, conduction, and analysis of the inspection. In this case, it is assumed, that the qualification of the involved personnel is sufficient, the functionality of the measuring equipment including the piezo elements is given, and the air temperature is within the permissible range, so that the oscillation and decay processes are not affected by unintended changes in the damping behaviour of the probes. In addition, a symmetrical zero-phase digital filter needs to be used so that filtering does not lead to phase shifting.

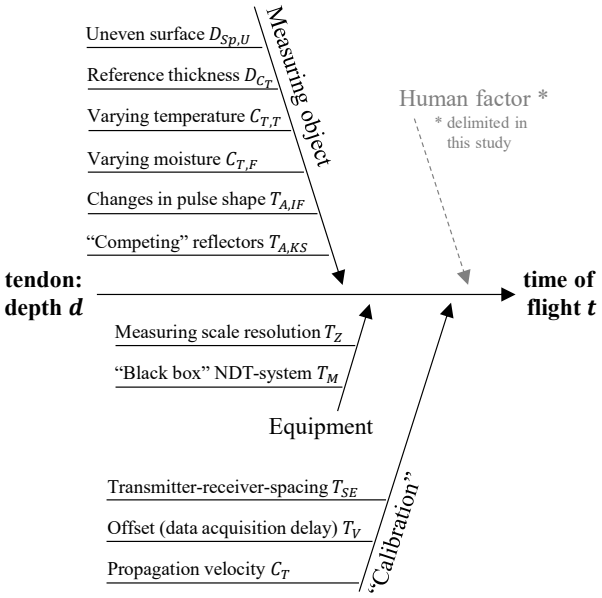

Fig. 5. Ishikawa diagram summarizing the input quantities

Some further input quantities are neglected in this particular case, but are considered potentially relevant in other inspection scenarios. The first quantity concerns signal processing using the Synthetic Aperture Focusing Technique (SAFT). SAFT assumes ideally point-shaped reflectors with a negligible diameter that are surrounded by a homogeneous-isotropic medium. In reconstruction of curved reflectors like tendons, the first assumption is not unrestrictedly admissible, since their comparatively large diameter may lead to different points of reflection when the measuring position is changed. As a result, the diffraction hyperbola may deviate from a hyperbola that could be expected at an ideal point-scatterer. In addition to a defocused tendon indication, this may cause a shift of the indication by a few millimetres compared to the raw data [28].

External interference signals whose frequencies lie within the bandwidth of the probe and therefore may not be filtered out for physical reasons can also contribute to uncertainty. Further, the dedicated segmentation of the pulse shape changes according to the causes, i.e., scattering, absorption, and dispersion might be useful.

Further uncertainties may arise, e.g., if the volume investigated to determine the sound velocity does not sufficiently correspond to the volume of interest with regard to material properties (such s concrete density) or secondary components (reinforcement, etc.). In practice, the sound velocity determination on drill cores may also result in systematic errors especially in the case of small diameters, i. a., because the sound velocity depends on the Poisson's ratio of the measuring object and different occurring wave types may cause errors in data analysis. In the case of components with inclined back walls, the angle of the reconstructed back wall can differ from the actual angle which would yield a higher uncertainty in sound velocity estimation. In other scenarios it might be necessary to differentiate some of the input quantities according to the testing task, i.e., whether the tendon is to be localized (Eqs. 1, 3) or the velocity is to be calibrated (Eq. 2), e.g., if the component thickness differs noticeably from the tendon mounting depths.

3.4 Case-study: Prestressed concrete bridge

3.4.1 Individual quantification of input quantities

The directly measurable quantities identified in sect. 3.2 were modelled to analyse the inspections on the bridge briefly outlined in section 3.1. The stochastic models are based on statistical analyses of measurements conducted under comparable boundary conditions in the lab ("Type A (Lab) evaluation"), on non-statistical methods (Type B) such as physical reasoning, or on the analysis of the on-site TOF measurements ("Type A (on-site)"). The mentioned evaluation methods yield equivalent results. Type B evaluation may be particularly useful if the sample size would be too small, or when the respective phenomenon can be explained very well ("extensive knowledge may obviate the need for measurements"). The results are given in Tables 1 and 2. Table 2 contains the input quantities that explicitly and strictly refer to the testing evaluated subsequently in section 3.4.2. Table 1 consists of the input quantities that may be used to guide future comparable measurement uncertainty calculation provided that the suitability of the models was carefully verified. Adjusting *some* models can be sufficient. Notes on correlation are delimited. The individual correlations were estimated for Type A evaluated quantities using the empirical covariance. Detailed information about the modelling of the quantities is provided in [11]. Chosen issues in individual quantification are discussed below.

In type A evaluation, parameters of the population are inferred from the sample using estimators. Given a sufficient number of independent, identically distributed observations, a normal distribution is often considered a good modelling approach (cf. central limit theorem). In type B, the distribution type is chosen "subjectively" on the basis of all available information. From the principle of maximum entropy, it can be concluded, e.g., that the uniform distribution may be suitable if it is solely known within which limits a random variable will be realized.

Consider exemplarily the **time axis resolution** T_Z limited due to a finite sampling rate. Given $f_s = 1\ MHz$, the delta between two samples is $1\ \mu s$ (which approx. equals to 2,7 mm impulse travel path). A measured value falls *arbitrarily* into an interval symmetrically spanned around a sample, with boundaries corresponding to half the distance between two samples. From this it follows that $T_Z \sim U$ with the limits $\pm 0{,}5\ \mu s$.

The second example concerns the **changes in pulse shape** $T_{A,IF}$, which lead to systematic errors in picking time stamps especially for reference points of an echo that are further away from the first arrival. The extent of these deviations depends on the frequency band, travel path, aggregate size, and water cement ratio. The bias is to be estimated and corrected to obtain true (cf. Fig. 1) times of flight. The measurement results published in i. a. [20–22] are applied to the specific modelling problem. A comprehensive empirical study will follow, since the uncertainties currently associated with the estimates of the systematic errors based on the available information are comparatively sizeable. This leads to the uncertainty contribution of $T_{A,IF}$ being the largest ($\approx 53\,\%$ [11]). The mean of the related random variable was estimated based on the shifts between the maxima of the envelope and the first arrival observed in [20, 21, 29] for different centre frequencies and travel paths between 10 cm and 90 cm to calculate a bias which at least roughly fits the expected mounting depths of the tendons between 15 cm and 40 cm in transversal bridge direction. It should be noted that the current data situation is insufficient for precise estimates. The standard uncertainty attributed to the bias is a combination of uncertainties arising from the lack of empirical results, varying concrete densities and the influence of the aggregate diameters.

The **delay** T_V depends mostly on the used equipment and can be measured comprehensively under laboratory condition. Reference specimens made of polyamide [30] and concrete were used to obtain the differences in time between backwall echoes and corresponding multiple reflections for different reference points such as the maximum of the signal envelope. The uncertainty of the bias ($\hat{t}_v = 27{,}83\ \mu s$) is $u(\hat{t}_V) = 0{,}33\ \mu s$ and therewith not decisive in measurement uncertainty calculation due to the large sample size with 1.938 time stamps picked for the backwall and 1.392 picked for the first multiple reflection which, together with simulation results, also justifies the choice of the normal distribution [11].

Table 1. Stochastic models of the input quantities quantified for the boundary conditions found at the individual structure.

Quantity X_i	Distr. type*	Mean $\hat{x}_i$	Stand. meas. unc. $u(\hat{x}_i)$	Type
$D_{Sp,U}$	U	0 cm	0,29 cm	B
$T_{A,IF}$	U	4,1 μs	5,8 μs	B
T_V	N	27,83 μs	0,33 μs	A (Lab)
T_Z	U	0 μs	0,29 μs	B
$C_{T,T}$	U	0 ms^{-1}	9 ms^{-1}	B
$C_{T,F}$	const.	0 ms^{-1}	0 ms^{-1}	B
$T_{A,KS}$	U	2 μs	1,16 μs	B
T_{SE}	const.	depends on depth position	0 μs	B
T_M	const.	0 μs	0 μs	A (Lab)

* N = Gaussian distribution; U = Uniform distribution

Table 2. Stochastic models of the input quantities quantified strictly for the considered individual structure and inspection.

Quantity X_i	Distr. Type	Mean $\hat{x}_i$ **	Stand. meas. unc. $u(\hat{x}_i)$	Type
D_{C_T}*	U	32,7 cm	0,58 cm	B
$T_{C_T,A}$*	N	$\approx$ 225 μs	$\approx$ 0,2 μs	A (on-site)
T_A*	N	$\approx$ 105 μs	$\approx$ 0,3 μs	A (on-site)

* Values observed in cross-section centre (y = 0 cm), cf. Figs. 6 & 7
** Mean values depend on x- & y-position

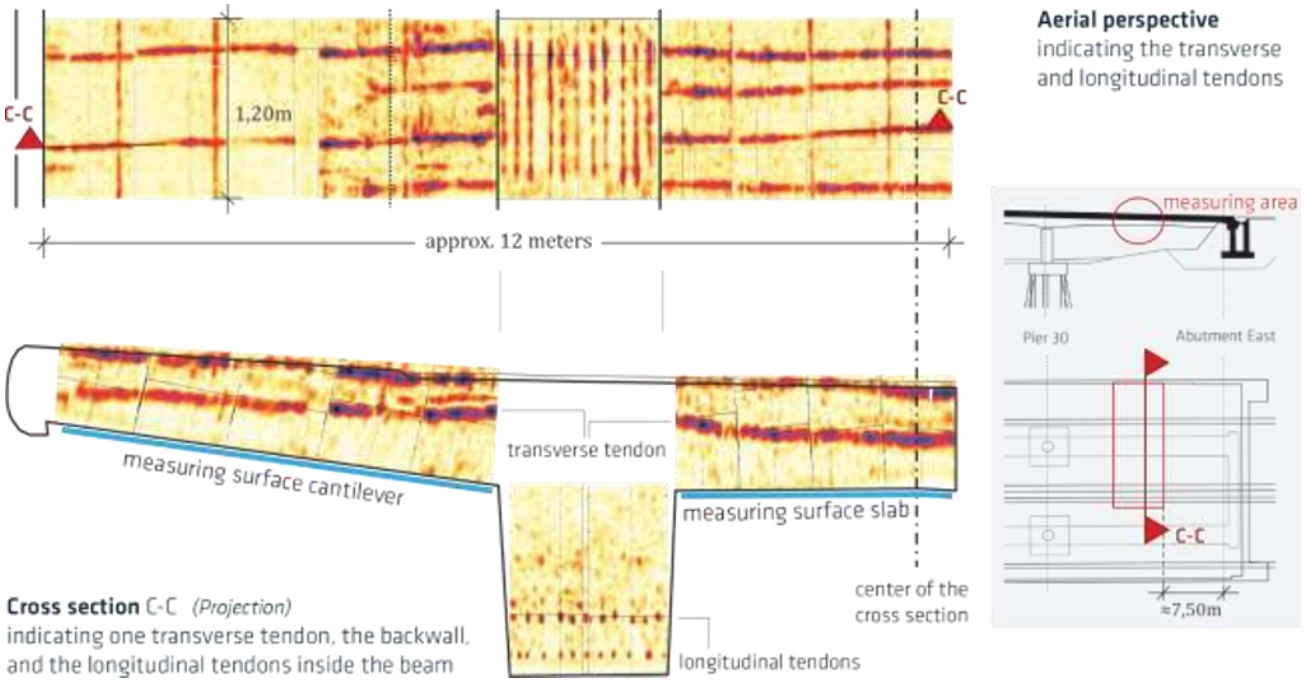

Fig. 6. Imaging of the ultrasonic data acquired at the concrete bridge with indications of the tendons. Extracted from [17], rearranged.

The fourth example is the **component temperature** $C_{T,T}$ varying spatially and temporally and affecting the sound velocity. The first assumption is a velocity change of $-1\ \% / 20\ K$ [19]. The second concerns the variation in the temperature of the investigated concrete slab. The national codes specify air temperatures between -24 °C and 37 °C for a reference period of 50 a [31]. Narrower intervals were determined in [32]. Considering the short measuring period of a week, a maximum variation of the mean component temperature of less than $\Delta T = 20\ K$ is expected, which might also cover temperature gradients. Based on these assumptions, the limits of a uniform distribution were specified to be $\pm 0{,}5\ \% / \pm 10\ K$. With $C_T \approx 3.000\ ms^{-1}$, the boundaries result in $\pm 15\ ms^{-1}$ per $\Delta T = \pm 10\ K$. From $u(\hat{x}_i) = \frac{b-a}{2\sqrt{3}}$ with a, b being the boundary values of a uniform distribution it follows that $u(\hat{c}_{T,T}) = \frac{30\ ms^{-1}}{2\sqrt{3}} \approx 9\ ms^{-1}$.

This paper only attempts to give some impressions on the modelling process. Please refer to [11] for details.

3.4.2 Imaging and measurement results

The ultrasonic echo data gathered on the concrete bridge was filtered ($5\ kHz < f < 100\ kHz$) and subsequently reconstructed using SAFT. Two extracted images, i.e., a cross section showing the curve of a transversal tendon in the slab and longitudinal tendons running through the main girder perpendicularly, as well as a depth section spanned over the varying vertical tendon positions are shown in Fig. 6. With the aim of using the measured locations of the transverse tendons in an NDT-based structural reliability analysis, the proposed measurement model was applied to convert the "coloured voxels" into quantitative measurement results. Inserting the best estimates of the input quantities (cf. means in Tables 1 and 2) into the model equations (Eqs. 1 – 3) yields the best estimate of the measurand for the position y = 0 cm (centre of the cross-section), that is the vertical position of one representative transversal tendon. The results for this and some further positions in y-direction, which were derived using the respective TOFs measured at the different measuring positions, are plotted in Fig. 7.

The combined standard measurement uncertainty to be attributed to these measured values is computed acc. to GUM using the Gaussian error propagation law and takes on values between $u(\hat{d}_{Sp}) = 6\ mm \ldots 7\ mm$. We can derive that the interval $\hat{d}_{Sp} \pm u(\hat{d}_{Sp})$ contains the value of interest with a probability of about 68 %, since the measurand is modelled using a normal distribution, which has been verified with Monte Carlo simulations.

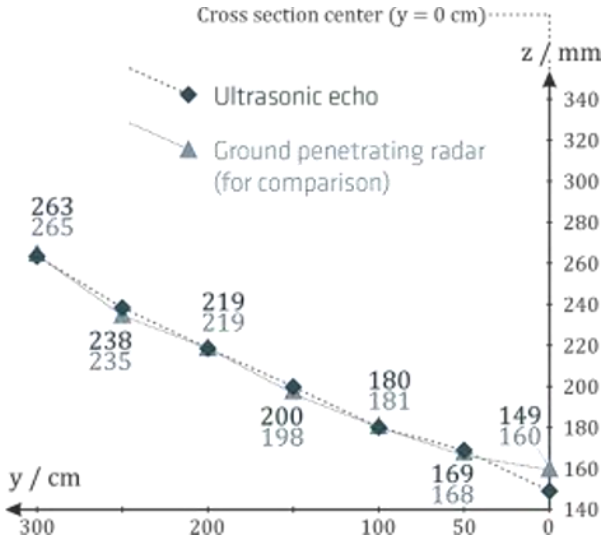

Fig. 7. Measured quantity values $\hat{d}_{Sp}$ for the mounting depths of one transversal tendon in relation to the bottom of the slab. Extracted from [11], translated, in excerpts.

3.4.3 Incorporation into reliability assessment

During its reassessment, the bridge has been verified in serviceability limit state decompression using the limit state function

$$g = 0 - \frac{\Theta_{E,N} \cdot \sum N_i}{h \cdot b} - \frac{\Theta_{E,M}\left(N_p \cdot z_p + \sum M_i\right)}{\frac{h^3 b}{12}} \cdot \frac{h}{2}, \qquad (4)$$

where $\Theta_{E,i}$ are the model uncertainties, N_i and M_i the different normal forces and bending moments computed with finite element analyses, and h, b the geometrical dimensions. The reliability analysis was performed via First Order Reliability Method (FORM). The stochastic models can be taken from [17]. The lever arm z_p is the vertical spacing between the cross-section centre and the strands and can be written as a function of the distance between the bottom of the slab and the tendon ducts d_{Sp} and the eccentricity of the strands inside the duct ϵ:

$$z_p = -\frac{h}{2} + d_{Sp} + \epsilon \qquad (5)$$

Decompression was verified in transversal direction and in the cross-section centre (y = 0 cm) using a one-meter strip (b = 1 m). This cross-section has been found to be decisive in prior finite element analyses. On the one hand, the measurements were intended to validate the assumptions according to the as-built documents. On the other, sensitivity analyses revealed that the vertical tendon duct position significantly influences reliability ($\alpha_{d_{Sp}}{}^2 \approx 50\,\%$). This notable relevance motivated the non-destructive localization of the transverse tendons.

Initially and prior to any testing, the vertical tendon position was modelled using a normal distribution with $\sigma = 1\ cm$ [33] and $\mu = 16{,}3\ cm$ according to the plans. The measurement result, in turn, is $d_{Sp} \sim N$ with a mean $\mu \triangleq \hat{d}_{Sp} = 14{,}9\ cm$ and a standard deviation σ which equals $u(\hat{d}_{Sp}) = 0{,}6\ cm$. Accordingly, a comparably slight but nevertheless mathematically unfavourable deviation between planned and measured (actual) position could be detected and the uncertainty reduced. The effects of including the measurement result instead of the initial model on the computational reliability are plotted in Fig. 8. The change in reliability index remains insignificant. However, the level of approximation of the computation model could be increased.

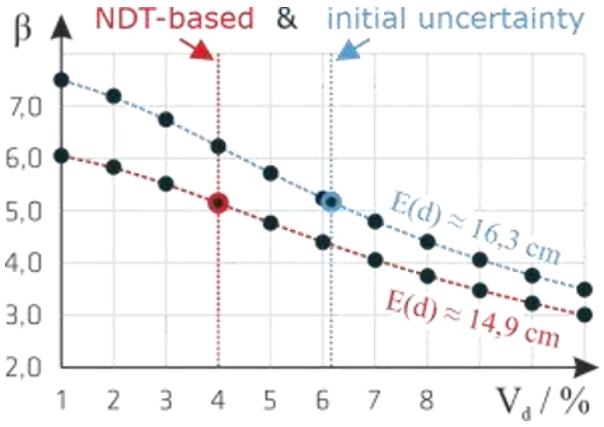

Fig. 8. Computed reliability index acc. to Hasofer/Lind over the coefficient of variation of the vertical tendon position for both expected values. Extracted from [11], translated, edited.

Overall, only chosen parts of the assessment process have been addressed in the present paper in order to show that non-destructive testing can also be utilized as a quality-assured tool to verify assumptions in reliability assessment and to facilitate more realistic structural analyses of existing structures. Further information can be found in [17].

4 Conclusion and outlook

This contribution provides a measurement model that has been used to quantify the quality, i.e., measurement uncertainty, of the localization of tendons in a specific prestressed concrete bridge using the ultrasound echo technique. This model may be used as a starting point for comparable inspections in the future. However, the suitability of the model must be thoroughly verified in each individual case and (some of) the input quantities might be re-quantified to achieve adequate results.

In subsequent research, the aim is to combine the advantages of the semi-probabilistic and probabilistic assessment concepts. Although probabilistic methods allow for the explicit consideration of measured data, computed failure probabilities are in many cases rather difficult to compare. In addition, their application may require more extensive theoretical knowledge. A semi-probabilistic assessment, in turn, is comparatively easily applicable and yields comparable computation results. Therefore, modified, i.e., structure-related, NDT-based, partial safety factors are intended to be derived. In this way, the engineer will be spared the “detour” via the probabilistic reliability analysis when he or she wants to use measured information on the structure directly for his or her assessment. Further, a systematic variation of boundary conditions during on-site inspections enables the development of a “net” consisting of approximate values of measurement uncertainties commonly to be expected on concrete structures for different testing tasks and measurement procedures. This facilitates to communicate efficiently which orders of magnitude of partial safety factor reduction the user can expect when certain measurement data is intended to be included in semi-probabilistic assessment of existing structures.

References

1. G. Marzahn, *Die Tragfähigkeitsreserven vieler älterer Brücken sind weitgehend aufgebraucht*: *Zur Weiterentwicklung der Nachrechnungsrichtlinie für die Entscheidung über Verstärkung oder Ersatz*, Der Prüfingenieur, 20 (2013)
2. Rechnungshof Rheinland-Pfalz, Bericht nach § 111 Abs. 1 LHO über die Erhaltung und den Zustand von Brücken in kommunaler Baulast: Az.: 2-P-0057-39-1/2011. Az.: 2-P-0057-39-1/2011, 2013
3. S. Maack, N. Diersch, Einsatz von zerstörungsfreien Prüfverfahren (ZfP-Verfahren) zur Rekonstruktion von Bestandsplänen als Grundlage für die Nachrechnung: Schlussbericht für das Forschungsprojekt FE 29.0333/2013/BASt. Schlussbericht für das Forschungsprojekt FE 29.0333/2013/BASt, 2015

4. K. Bergmeister, *Monitoring and safety evaluation of existing concrete structures*: *State-of-art report prepared by Task Group 5.1* (fib, Lausanne, 2003)
5. J. Fischer, D. Straub, R. Schneider, S. Thöns, W. Rücker, *Intelligente Brücke - zuverlässigkeitsbasierte Bewertung von Brückenbauwerken unter Berücksichtigung von Inspektions- und Überwachungsergebnissen* (Fachverlag NW, Bremen, 2014)
6. C. Maierhofer, H.-W. Reinhardt, G. Dobmann, eds., *Non-Destructive Evaluation of Reinforced Concrete Structures*: *Volume 2: Non-Destructive Testing Methods* (Woodhead Publishing, Cambridge, UK, 2010)
7. Joint Committee for Guides in Metrology, *JCGM 100:2008. Evaluation of measurement data — Guide to the expression of uncertainty in measurement* (2008) (2008)
8. Joint Committee for Guides in Metrology, *JCGM 101:2008. Evaluation of measurement data — Supplement 1 to the "Guide to the expression of uncertainty in measurement" — Propagation of distributions using a Monte Carlo method* (2008) (2008)
9. Joint Committee for Guides in Metrology, *JCGM 102:2011. Evaluation of measurement data – Supplement 2 to the "Guide to the expression of uncertainty in measurement" – Extension to any number of output quantities* (2011) (2011)
10. Joint Committee for Guides in Metrology, *JCGM GUM-6:2020. Guide to the expression of uncertainty in measurement — Part 6: Developing and using measurement models* (2020) (2020)
11. S. Küttenbaum, *Zur Validierung von zerstörungsfreien Messverfahren für die probabilistische Beurteilung von Bestandsbauwerken mit gemessenen Daten*, Dissertation, Universität der Bundeswehr München, 2021
12. M. Krystek, *Calculating measurement uncertainties*: *Basic principles and implementation* (Beuth, Berlin, Wien, Zürich, 2016)
13. W. Hässelbarth, Guide to the Evaluation of Measurement Uncertainty for Quantitative Test Results: EUROLAB Technical Report No. 1/2006. EUROLAB Technical Report No. 1/2006, 2006
14. Joint Committee for Guides in Metrology, *JCGM 200:2012. International vocabulary of metrology – Basic and general concepts and associated terms (VIM)*: *3rd edition* (2012) (2012)
15. A. Taffe, *Zur Validierung quantitativer zerstörungsfreier Prüfverfahren im Stahlbetonbau am Beispiel der Laufzeitmessung* (Beuth, Berlin, Wien u.a., 2008)
16. Joint Committee for Guides in Metrology, JCGM 104:2009. Evaluation of measurement data — An introduction to the "Guide to the expression of uncertainty in measurement" and related documents, 2009
17. S. Küttenbaum, T. Braml, A. Taffe, S. Keßler, S. Maack, *Reliability assessment of existing structures using results of nondestructive testing*, Structural Concrete **22**, 2895 (2021)
18. M. Krause, F. Mielentz, B. Milmann, D. Streicher, K. Mayer, *Ultrasonic reflection properties at interfaces between concrete steel and air: imaging and modelling*, In: Al-Quadi, I. and G. Washer (eds.); Proceedings of the NDE Conference on Civil Engineering, 14.-18.08.2006, St. Louis, MO, USA, 472 (2006)
19. E. Niederleithinger, *Seismic Methods Applied to Ultrasonic Testing in Civil Engineering*, Habilitationsschrift, RWTH, 2017
20. M. Schickert, M. Krause, Ultrasonic techniques for evaluation of reinforced concrete structures, in *Non-Destructive Evaluation of Reinforced Concrete Structures: Volume 2: Non-Destructive Testing Methods*, edited by C. Maierhofer, H.-W. Reinhardt, G. Dobmann (Woodhead Publishing, Cambridge, UK, 2010), 490
21. M. Schickert, M. Krause, W. Müller, *Ultrasonic Imaging of Concrete Elements Using Reconstruction by Synthetic Aperture Focusing Technique*, Journal of Materials in Civil Engineering **15**, 235 (2003)
22. S. Popovics, J. L. Rose, J. S. Popovics, *The Behavior of Ultrasonic Pulses in Concrete*, Cement and Concrete Research **20**, 259 (1990)
23. G. I. Crawford, Guide to Nondestructive Testing of Concrete, 1997
24. E. Niederleithinger, C. Wunderlich, Influence of small temperature variations on the ultrasonic velocity in concrete (AIP, 2013), 390
25. E. Ohdaira, N. Masuzawa, *Water content and its effect on ultrasound propagation in concrete — the possibility of NDE*, Ultrasonics **38**, 546 (2000)
26. S. Popovics, *Effects of uneven moisture distribution on the strength of and wave velocity in concrete*, Ultrasonics **43**, 429 (2005)
27. U. Lencis, A. Udris, A. Korjakins, *Moisture Effect on the Ultrasonic Pulse Velocity in Concrete Cured under Normal Conditions and at Elevated Temperature*, Construction Science **14** (2013)
28. S. Schulze, *Untersuchung von Spannbetonkonstruktionen mit bildgebenden Ultraschallecho-Verfahren*, Dissertation, Technische Universität, 2017
29. M. Schickert, Messtechnische Untersuchungen zur Charakterisierung der Ausbreitung von Ultraschall in Beton, in *Tagungsband zur DGZfP-Jahrestagung 2007*, edited by Deutsche Gesellschaft für Zerstörungsfreie Prüfung (DGZfP, Berlin, 2007), V37-1-11
30. S. Maack, S. Küttenbaum, N. Epple, M. Aligholizadeh, *Die Ultraschall-Echomethode – von der Messung zur bautechnischen Kenngröße*, Beton- und Stahlbetonbau **116**, 200 (2021)
31. Deutsches Institut für Normung e. V., *DIN-Fachbericht 101: Einwirkungen auf Brücken* (Beuth, Berlin, 2009) (2009)
32. U. Lichte, *Klimatische Temperatureinwirkungen und Kombinationsregeln bei Brückenbauwerken*, Dissertation, Universität der Bundeswehr, 2004
33. JCSS, *Probabilistic Model Code*: *Part 1-3* (Joint Committee on Structural Safety, Zurich, 2001/2002)